Test Bench Characterisation and Frequency Domain Torsional Model Validation of Transmission Systems and Components

Test Bench Characterisation and Frequency Domain Torsional Model Validation of Transmission Systems and Components

E. Galvagno [*], A. Tota [†], M. Velardocchia [‡], A. Vigliani [§]
Dip. di Ingegneria Meccanica e Aerospaziale, Politecnico di Torino
Torino, Italy

Abstract— *The article presents an experimental methodology used to characterize the torsional dynamic behaviour of automotive transmission systems and components and the analytical methods for simulating them in the frequency domain.*

A general description of the test bench is given in the paper: it is composed of an induction motor for the torsional excitation of the system and of torque and angular position sensors. The tests were carried out by keeping one end of the transmission locked.

Two case study are discussed: a Dual Mass Flywheel (DMF) and a complete Automated Manual Transmission (AMT). In the first example the experimental data from sine sweep tests are used to estimate the damping factor of the DMF. In the second case the dependency of the frequency response function (FRF) on the engaged gear ratio for a 5-speed AMT is investigated. A torsional model for each test rig configuration is proposed and the corresponding equations of motion derived. The compliance FRFs of the torsional systems are then numerically evaluated and compared with the results from the experiments. A good match between simulated and measured data is shown.

Keywords: test bench measurements, experimental analysis, frequency response function, Dual Mass Flywheel, Automated Manual Transmission, torsional vibrations, mechanical system dynamics, frequency domain modelling, automotive, experimental modal analysis.

I. Introduction

The internal combustion engine is the main source of torsional vibrations on conventional passenger cars. The engine firing torque pulses, due to gas pressure, and the inertia imbalance torque, due to acceleration of reciprocating masses, torsionally excite the transmission dynamic system downstream of it.

In Manual Transmission powertrains, the growing demand for improving vibration isolation from the engine irregularities has led to a more and more widespread dissemination of the Dual Mass Flywheel as a torsional damper.

[*] enrico.galvagno@polito.it
[†] antonio.tota@polito.it
[‡] mauro.velardocchia@polito.it
[§] alessandro.vigliani@polito.it

It works as a mechanical low-pass filter for the vibrations coming from the engine and entering into the gearbox. As stated in [1], the dynamic performance of this component is not easily predictable from the technical specifications provided by DMF suppliers especially in terms of vibration damping around the resonance. Therefore experimental test bench characterisation remains an effective method to systematically investigate its dynamic behaviour under different operating conditions.

In [2] there is a detailed description of an experimental apparatus specially designed to examine the dynamic performance of a wide variety of torsional vibration absorber.

In [1] the torsional dynamic behaviour of a DMF is investigated both experimentally and numerically. An analytical expression for the frequency response function describing the rotational dynamics of the test rig is derived and compared with the estimate from experimental data.

Compared to the two approaches aforementioned, that used arbitrary waveform generators for the excitation of the dynamic system, a more sophisticated experimental technique, is Hardware-in-the-loop (see e.g. [3], [4] and [5]), that allows to test the component under more realistic loading conditions. Real-time simulation of the remaining part of the system, non physically present on the test bench, allows calculating a stimulus for the system that is closer to real-word conditions.

As a reference on the issues that must be considered in order to obtain accurate torsional measures see e.g. [6]. In that paper an overview of analogue and digital torsional vibration measurement method is presented. The errors associated with the digital measurements (e.g. encoder and magnetic pick-up) are discussed and methods to minimise measurement error (like aliasing, leakage, tooth spacing variation, etc.) are explored. Also in [7] several torsional vibration measurement techniques are presented, together with remarks on precautions

against possible sources of error, and the order of accuracy to be expected of the test results.

The experimental analysis of the torsional vibration of a complete AMT, from the dual mass flywheel to the wheel hub, is not yet present in the literature to the best of authors' knowledge. See e.g. [8] for further details on automated manual gearboxes and their components. This testing activity, that we have carried out and documented in this paper, has allowed to achieve the following objectives: to identify the damping effect due to gears rotation in the lubrication oil, to investigate the effect of the gear engaged on the frequency response function and to define a simplified 2-DOF torsional model able to describe the transmission system behaviour up to a maximum frequency of 30 Hz.

In this paper after a general description of the test rig used for the measurement and analysis of the torsional vibrations, the forcing function applied to the system during the tests and the system response are shown both in time and in time-frequency domain, by means of spectrogram plots. The method used to estimate the frequency response function from the input and output time histories is discussed and the resulting experimental FRF is shown. A 2-DOF linear torsional model for each system under test (DMF and AMT) is proposed and experimentally validated in the frequency domain. The classical approach for the computation of the FRF from the dynamic system matrices is extended to the case in which the measuring point of the excitation does not coincides with the exact point of application.

II. Test description and specifications

A. The torsional exciter system

A tri-phase asynchronous electric motor with a rated power of 11kW and a rated torque of 110 Nm, is the torsional exciter for the mechanical system under test.
The torque delivered by the electric motor is applied to one side of the transmission component (or system) while the other side is fixed to the frame of the test bench.
The electric motor drive is a frequency inverter set into vector control mode; during the tests the torque control mode is enabled since the electric motor is used to apply almost harmonic torque to the mechanical system.
The reference torque T_{ref} for the electric motor control system is a linear chirp, that is a constant amplitude sine wave whose frequency $f(t)$ varies linearly with time:

$$T_{ref} = T_m + T_0 \sin(2\pi f(t) \cdot t + \varphi_0) \qquad (1)$$

where T_m [Nm] is the torque mean value, T_0 [Nm] is the amplitude of the sine wave, φ_0 is the initial phase [rad], and $f(t)$ is the instantaneous sweep frequency [Hz]:

$$f(t) = f_0 + \frac{f_0 - f_1}{t_{chirp}} t \qquad (2)$$

f_0 is the starting frequency, f_1 is the final frequency and t_{chirp} is the duration of the chirp signal.
The generation of the analogue voltage proportional to the reference torque which is the setpoint for the motor drive was performed thorough a 13-bit waveform analogue output module.

B. The sensors

The time histories of the torque effectively produced by the electric motor and the angular position of its shaft are measured through the following sensors:

- a contactless torque transducer with a measuring range of ±230 Nm and accuracy class of 0.1% of full scale value measures the torque immediately downstream of the electric motor;
- a rotary incremental encoder with 1024 pulses per revolution is mounted on the rear side of the electric motor and allows to measures the angular position of the motor shaft with a resolution of ≈0.35°.

C. The transmission component and system under test

The same test bench was used, with minor modifications, to test a Dual Mass Flywheel and a 5-speed Automated Manual Transmission. Fig. 1 shows the pictures of the two test bench configurations.
In the first case (top) the torque generated by the electric motor is applied to the first mass of the flywheel, while the second mass is kept fixed to the frame of the rig. A special bearing support (S) for the flywheel was designed and integrated on the test bench.
The second experimental setup (bottom) includes the flywheel and its support, a clutch unit, a single-stage 5-speed gearbox having a torque capacity of 300 Nm, a half shaft, a wheel hub and a disk brake used to lock the transmission end. Also in this case the torque is applied by the induction motor to the first mass of the flywheel after being measured through the torque sensor.
The tested transmission has a primary shaft and a single secondary shaft. The differential has been locked in order to allow the usage of only one of the two half-shafts to transfer the mechanical power to the wheel hub of the bench. The transmission has three synchronisers: one for the 1st , 2nd and Reverse gear which is located on the secondary shaft, a second synchronisers for the 3rd and 4th gear and one for the 5th gear which are both mounted on the primary shaft. The lubrication system adopted is a splash lubrication with the differential gear almost completely immersed in the lubrication oil and gears on the secondary shaft dipping into the oil bath and

transferring the lubricant to the meshing teeth of the primary shaft as they rotates.

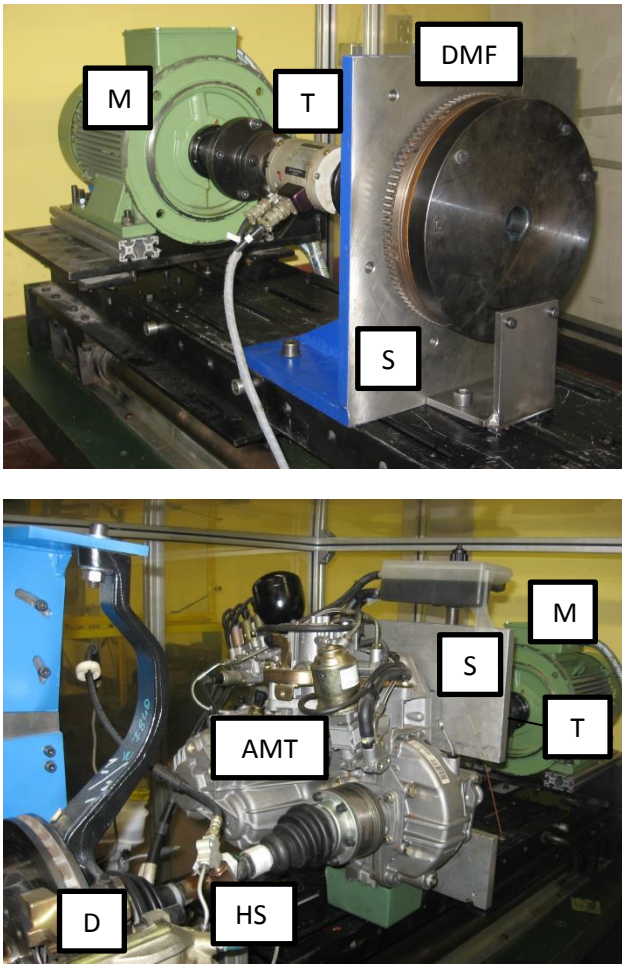

Fig. 1 – Test bench for DMF (top) and AMT (bottom) characterisation. M: electric motor, T: torque meter, S: bearing support, DMF: dual mass flywheel, AMT: automated manual transmission, HS: half shaft, D: disk brake.

III. Data acquisition and signal analysis

Raw data were acquired from the test bench's sensors at a sampling frequency of 10kHz through a *National Instruments*® data acquisition boards. An example of the original time histories of the measured torque and angular position is shown in Fig. 2; a linear torque sweep is applied to one end of the transmission system while the other end is locked.

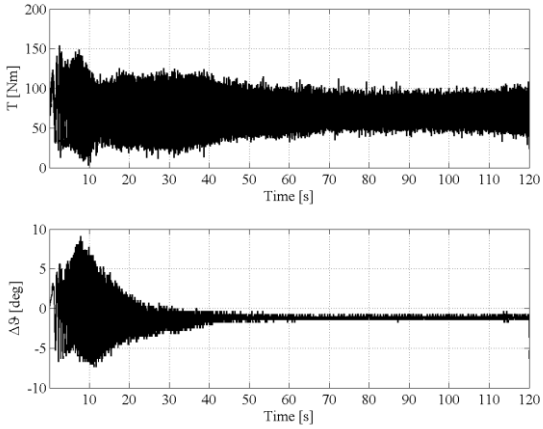

Fig. 2 - Time histories of the torque and angular position during a linear sweep test, from 0.1 to 80Hz.

Due to the transient nature of the test, it is convenient to analyse the measured signals in time-frequency domain. To this aim the two signals have been down-sampled by a decimation factor of 50 after being low pass filtered to avoid aliasing; then spectrograms have been calculated from the time signals as the magnitude of the short time Fourier transform (STFT).

The input parameters for the spectrogram algorithm are:

- windows type: Hamming;
- windows length: 2s;
- overlap between segment: 80%;
- sampling frequency: 200 Hz.

The spectrograms of the two signals expressed in decibel (dB) are shown in Fig. 3 and Fig. 4.

Observing the charts in Fig. 2 it can be pointed out at least qualitatively that, although the reference signal to the torque control of the electric motor has a constant amplitude, see eq.(1), the actual output torque has an amplitude that varies with the sweep frequency. Therefore it can be deducted that the frequency response of the torsional exciter is not simply a constant over the frequency range of interest. A method to solve this problem is described in [1], where the design of a feed-forward dynamic compensator is presented aiming at increasing the performance of a standard electric torque actuator to be used as a torsional exciter.

A further element of non-ideality of the torque generation system can be identified from Fig. 3, where, in addition to the fundamental frequency, higher harmonics occurring at whole-number multiples (2x, 3x, etc.) of the sweep frequency are clearly visible.

Moreover from Fig. 2 and Fig. 4 it can be seen that the response of the system after second 45 begins to be very attenuated so that the encoder resolution is no more adequate to measure the so small oscillation amplitudes. For this reason the investigation of the frequency response of the system is limited to a maximum frequency of 30 Hz.

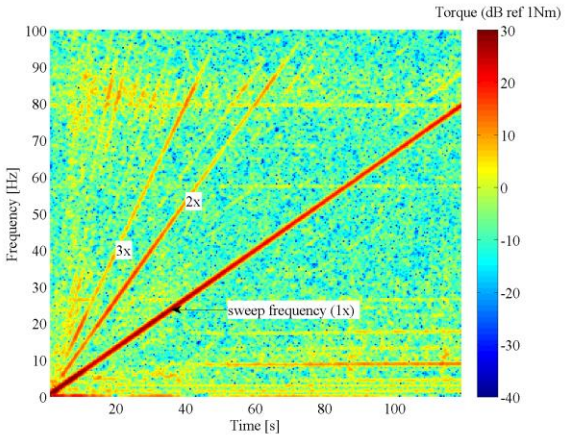

Fig. 3. Spectrogram of the measured torque during a linear chirp.

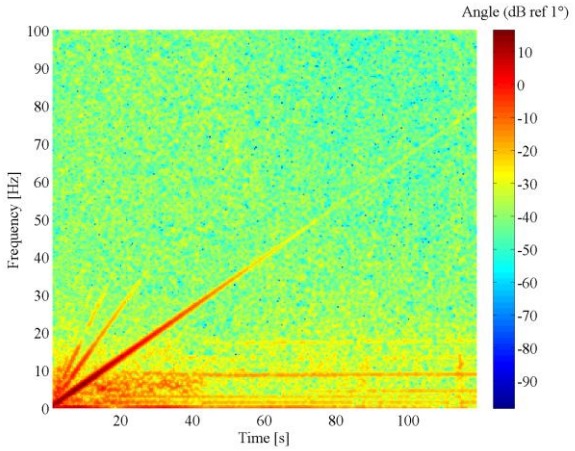

Fig. 4 Spectrogram of the measured angular displacement during a linear chirp.

IV. Experimental transfer function estimation

Considering small oscillation around the static equilibrium position, a linear time-invariant transfer function can be used to model the relationship between the input (x=Torque) and output (y=Angle).
Since the vibration response is measured in terms of displacement, the FRF represents a compliance function.
Due to the digital nature of the encoder measure it is assumed that the noise in the output signal is negligible, therefore the unknown transfer function is estimated using the so-called H_2 estimator [9], that is the quotient of the auto power spectral density of the output $P_{yy}(f)$ and the cross power spectral density between output and input $P_{yx}(f)$

$$H_2(f) = \frac{P_{yy}(f)}{P_{yx}(f)} \tag{3}$$

To evaluate the quality of the estimated FRF the coherence function is also computed:

$$C_{xy}(f) = \frac{|P_{xy}(f)|^2}{P_{xx}(f)\,P_{yy}(f)} \tag{4}$$

where $P_{xx}(f)$ is the auto power spectral density of the input and $P_{xy}(f)$ is the cross power spectral density between input and output.
The algorithm for finding the transfer function and coherence function estimates given experimental input and output signal vectors uses the Welch's averaged periodogram method [9]. The input parameters for the transfer function estimation algorithm are: Hamming window type; 2 second window length; 80% overlap between segment and 200 Hz sampling frequency.

A. *Case study #1: the DMF*

The amplitude and phase of the estimated transfer function and the coherence function computed using the time signals previously commented are shown in Fig. 5.

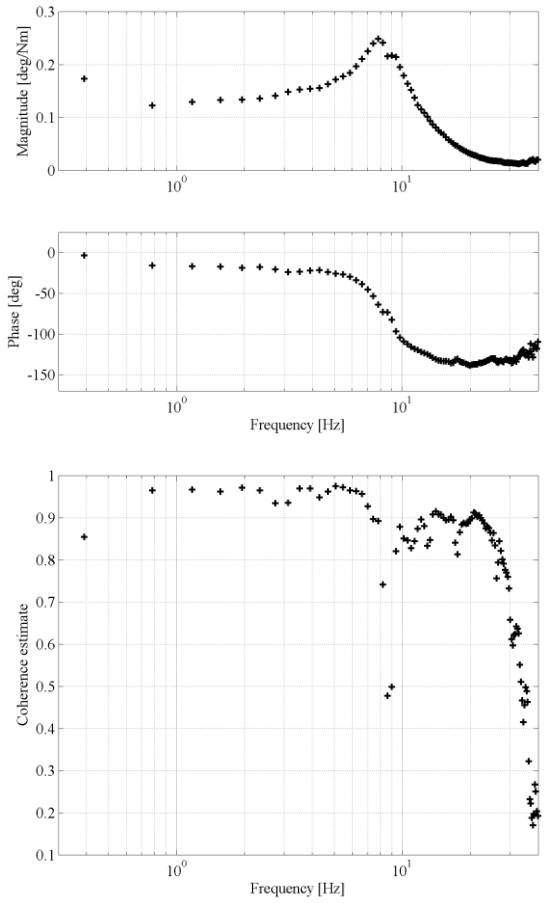

Fig. 5 Transfer function estimate (top) from 0.3Hz to 40 Hz using H_2 estimator and the coherence function (bottom).

The amplitude of the experimental FRF has a unique peak at about 8 Hz in the considered frequency range; at that frequency the phase is -64°. Looking at the coherence function it should be noted that the accuracy of the estimate for frequency higher than 30 Hz and in a

narrow band to the right of the peak frequency is poor, while elsewhere the quality of the estimate is satisfactory.

B. Case study #2: the AMT

The same computational methods illustrated for the DMF are used for the estimation of the frequency response function of a complete Automated Manual Transmission (AMT). Separate sweep tests were performed for each gear engaged, from 2nd to 5th gear, and the estimated transfer functions are compared in Fig. 6.

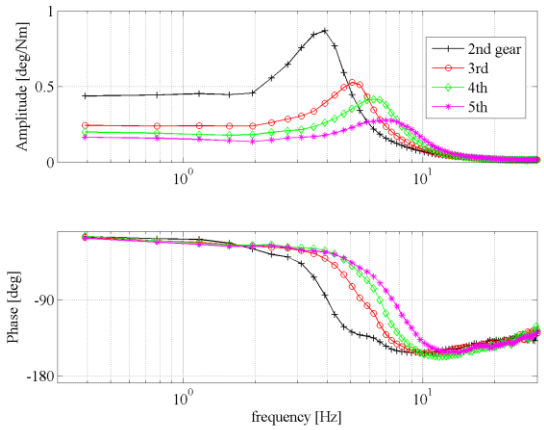

Fig. 6 Transfer function estimates, modulus (top) and phase (bottom), for different gear engaged in the AMT.

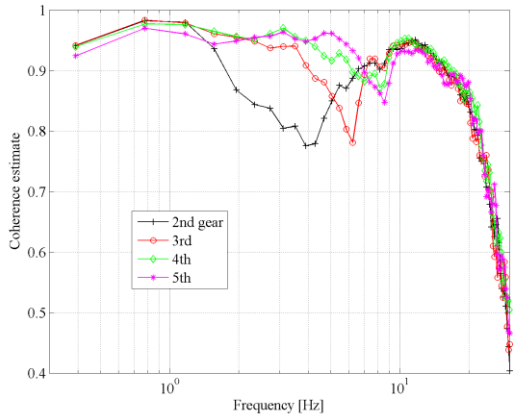

Fig. 7 Coherence function estimates for the tests with different gear engaged in the AMT.

Also in this case the amplitude of each experimental FRF has only one resonance peak in the considered frequency range. The coherence function in Fig. 7 indicates that the accuracy of the estimate is high up to 20Hz, from that frequency forward the coherence drops below 0.8.

The comparison shows that the resonance frequency increases as the gear engaged, i.e. passing from the second to the fifth speed the peak frequency changes from 4 to 7 Hz, gaining about 1 Hz for each gear change. The DC gain decreases passing from 0.44 °/Nm in 2nd gear to 0.16 °/Nm in 5th gear mainly due to the different gear ratio imposed by the engaged synchroniser. In fact the ratio between the DC gains obtained during tests with two different engaged gears is approximately equal to the ratio between the two gear ratios:

$$\frac{H_2(f=0)|_{gear\,i}}{H_2(f=0)|_{gear\,j}} \cong \frac{\tau_i}{\tau_j} \tag{5}$$

The phase lag progressively increases from about 15° at 0.4 Hz to 150° at 12 Hz, while for frequencies higher than 12 Hz the phase lag begins to decrease. The major differences between the curves in terms of phase are concentrated in the neighbourhood of the resonance frequency.

V. Torsional model and numerical transfer functions

A. Case study #1: the DMF

Starting from the free body diagrams illustrated in Fig. 8 the dynamic balance equations for the two degree of freedom (d.o.f.) system can be easily found:

$$\begin{cases} I_1\ddot{\vartheta}_1 + c_1(\dot{\vartheta}_1 - \dot{\vartheta}_2) + k_1(\vartheta_1 - \vartheta_2) + c_M\dot{\vartheta}_1 = T_M \\ I_2\ddot{\vartheta}_2 - c_1(\dot{\vartheta}_1 - \dot{\vartheta}_2) - k_1(\vartheta_1 - \vartheta_2) + c_2\dot{\vartheta}_2 + c_B\dot{\vartheta}_2 = 0 \end{cases} \tag{6}$$

where $I_1 = I_M + \frac{I_T}{2}$; $I_2 = \frac{I_T}{2} + I_S + I_{F1}$

I_M, I_T, I_S and I_{F1} are mass moments of the inertia of: the rotor of the electric motor, the torque meter, the rotating shaft for the connection of the torque meter to the primary mass of the DMF, the primary mass of the DMF respectively;
(since the secondary mass of the DMF is locked it does not appear in the equations of motion)

c_1, c_2, c_M and c_B are viscous damping coefficients of: the torque meter, the internal dissipation of dual mass flywheel, the motor bearings and the bearing system supporting the input shaft connected to the DMF;

k_1 is the torsional stiffness of the DMF;

T_M is the electromagnetic torque of the electric motor, the excitation for the dynamic system.

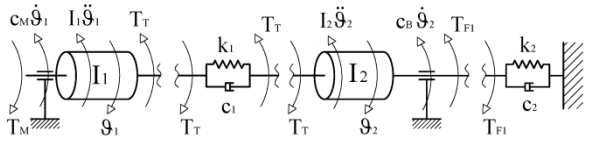

Fig. 8 – Free body diagrams of the test rig rotating parts for the torsional analysis of the Dual Mass Flywheel.

The equations of motion of the torsional system can be cast in matrix form:

$$\begin{bmatrix} I_1 & 0 \\ 0 & I_2 \end{bmatrix}\begin{Bmatrix} \ddot{\vartheta}_1 \\ \ddot{\vartheta}_2 \end{Bmatrix} + \begin{bmatrix} c_1 + c_M & -c_1 \\ -c_1 & c_1 + c_2 + c_B \end{bmatrix}\begin{Bmatrix} \dot{\vartheta}_1 \\ \dot{\vartheta}_2 \end{Bmatrix} + \\ + \begin{bmatrix} k_1 & -k_1 \\ -k_1 & k_1 + k_2 \end{bmatrix}\begin{Bmatrix} \vartheta_1 \\ \vartheta_2 \end{Bmatrix} = \begin{Bmatrix} T_M \\ 0 \end{Bmatrix} \quad (7)$$

Recalling that the experimentally estimated FRF is the ratio between the two measured quantities, i.e. the angular position of the electric motor ϑ_1 and the torque sensed by the torque transducer T_T, it is therefore necessary to derive the mathematical relationship between these two variables in order to allows the comparison between experimental and model results.
The receptance method, see e.g. [10] for details, is a useful instrument to calculate the steady state response of a M-DOF (multi-degrees of freedom) system to harmonic excitations applied to a system DOF. To allow the application of this method it is necessary to express the ratio between output and input quantity as a function of the external torque applied to a specific degree of freedom. In this case, the external action for the torsional dynamic system that is applied to the motor inertia, the first system DOF, is the electromagnetic motor torque T_M:

$$\frac{\vartheta_1}{T_T} = \left(\frac{\vartheta_1}{T_M}\right)\cdot\left(\frac{T_M}{T_T}\right) = \left(\frac{\vartheta_1}{T_M}\right)\cdot\left(\frac{T_T}{T_M}\right)^{-1} \quad (8)$$

The torque meter torque T_T must be derived as a linear combination of the system input (T_M), the generalized coordinates and their time derivatives. To this aim the dynamic balance of the torques applied to the first inertia gives:

$$T_T = T_M - I_1\ddot{\vartheta}_1 - c_M\dot{\vartheta}_1 \quad (9)$$

Dividing both sides of the equation by the motor torque T_M it yields:

$$\frac{T_T}{T_M} = 1 - I_1\frac{\ddot{\vartheta}_1}{T_M} - c_M\frac{\dot{\vartheta}_1}{T_M} \quad (10)$$

Under harmonic regime of motion in the right end side of the former equation the derivatives with respect to time can be expressed as a function of the frequency of oscillation Ω:

$$\begin{cases} \frac{\ddot{\vartheta}_1}{T_M} = -\Omega^2\frac{\vartheta_1}{T_M} \\ \frac{\dot{\vartheta}_1}{T_M} = j\Omega\frac{\vartheta_1}{T_M} \end{cases} \quad (11)$$

Hence, inserting eq. (11) into (10) the transfer function between the measured torque and the motor torque is:

$$\frac{T_T}{T_M} = 1 + I_1\Omega^2\frac{\vartheta_1}{T_M} - c_M j\Omega\frac{\vartheta_1}{T_M} \quad (12)$$

Finally, substituting eq.(12) in (8) the requested transfer function is:

$$\frac{\vartheta_1}{T_T} = \left(\frac{\vartheta_1}{T_M}\right)\cdot\left(1 + I_1\Omega^2\frac{\vartheta_1}{T_M} - c_M j\Omega\frac{\vartheta_1}{T_M}\right)^{-1} \quad (13)$$

Where the transfer function $\frac{\vartheta_1}{T_M}$ can be calculated through the inversion of the dynamic stiffness matrix, as explained in the next steps.

Considering harmonic excitation applied to the motor inertia the equation of motion becomes:

$$[I]\{\ddot{\vartheta}\} + [C]\{\dot{\vartheta}\} + [K]\{\vartheta\} = T_{M0}\{1 \quad 0\}^T e^{j\Omega t} \quad (14)$$

where T_{M0} is the amplitude of the motor torque and Ω is the frequency of the harmonic excitation.

The steady-state response of the linear 2 DOF system is also harmonic:

$$\begin{cases} \{\vartheta(t)\} = \{\Theta_0\}\, e^{j\Omega t} \\ \{\dot{\vartheta}(t)\} = j\Omega\,\{\Theta_0\}\, e^{j\Omega t} \\ \{\ddot{\vartheta}(t)\} = -\Omega^2\,\{\Theta_0\}\, e^{j\Omega t} \end{cases} \quad (15)$$

where $\{\Theta_0\}$ is a 2x1 complex vector.

Substituting eq.(15) in eq.(14), the steady state response amplitude is:

$$\{\Theta_0\} = [G(j\Omega)]\, T_{M0}\{1 \quad 0\}^T \quad (16)$$

Where $[G(j\Omega)]$ is the receptance matrix or frequency response function matrix, that is the inverse of the dynamic stiffness matrix $\left[K_{dyn}(\Omega)\right]$:

$$[G(j\Omega)] = \left[K_{dyn}\right]^{-1} = ([K] - \Omega^2[I] + j\Omega[C])^{-1} \qquad (17)$$

The first element on the main diagonal, i.e. $G_{1,1}(j\Omega)$, is the transfer function we are looking for, linking the amplitude of excitation applied at the motor inertia to the amplitude of the system response, i.e. the angular displacement of the motor rotor.

$$\Theta_{10} = G_{1,1}(j\Omega)\, T_{M0} \qquad (18)$$

Substituting eq. (18) in eq. (13) the requested transfer function can be evaluated.

B. Case study #2: the AMT

A simplified linear dynamic model for the study of the torsional vibration of an AMT up to 30 Hz is proposed in Fig. 9.

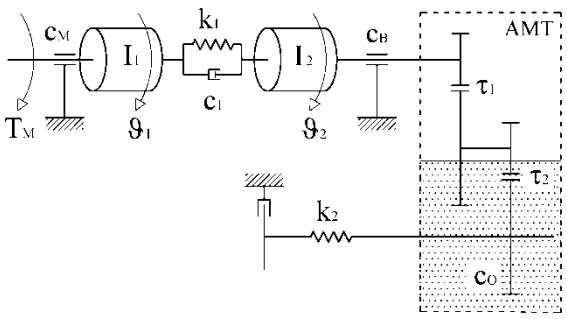

Fig. 9 – Torsional model of the test rig rotating parts for the dynamic analysis of the AMT.

In contrast to what was done for the DMF model, where also the torque meter compliance was taken into account, in the AMT model the torque meter is considered infinitely stiff and the system compliance is concentrated in other two points, the DMF (arc springs) with stiffness k_1 and the half shaft with stiffness k_2.

A single lumped inertia I_1 is used to account for the inertial properties of the rotating components from the rotor of the electric motor to the first mass of the flywheel. Then a spring and a viscous damper element represents the elastic and dissipative effect of the DMF and the second inertia I_2 models the second mass of the flywheel and the equivalent inertia of the transmission. The gearbox is considered infinitely stiff and an ideal model of gears, with a set of selectable gear ratios $\tau_i = \tau_1\tau_2$ and unitary efficiency, represents the speed reduction and torque amplification effect of the gearbox. A spring element models the half shaft compliance.

A separate discussion must be done for the damping effect of the gearbox. Due to the fact that several gears are immersed at least partially in the lubrication oil, the rotation of these gears originates a viscous damping torque opposing the direction of rotation and therefore increasing the energy dissipation. Therefore, the efficacy of the transmission oil to dampen the torsional vibration of the system must not be neglected.

This damping effect can be split into two contributions:

a. the drag torques applied to the idle gears on the secondary shaft in constant mesh with the gears fixed to the primary shaft, i.e. the 1st, 2nd and Reverse gear;

b. the drag torques applied to the gears connected to secondary shaft, i.e. the 3rd , 4th and 5th , and the differential gears.

The first contribution is modelled through a linear viscous damper applied to the primary shaft. A unique damping coefficient c_B is implemented in the model, representing the effect of both the bearing support for the flywheel and the contribution of the gearbox just introduced.

The second damping contribution in the gearbox is modelled as another viscous damper (damping coefficient: c_O) this time applied to the output shaft of the transmission.

The excitation is applied by the electric motor to the input side of the transmission while the other end is locked by means of a disk brake.

The equations of motion of the AMT torsional system in matrix form are:

$$\begin{bmatrix} I_1 & 0 \\ 0 & I_2 \end{bmatrix}\begin{Bmatrix} \ddot{\vartheta}_1 \\ \ddot{\vartheta}_2 \end{Bmatrix} + \begin{bmatrix} c_1 + c_M & -c_1 \\ -c_1 & c_1 + c_B + c_O/\tau^2 \end{bmatrix}\begin{Bmatrix} \dot{\vartheta}_1 \\ \dot{\vartheta}_2 \end{Bmatrix} + \\ + \begin{bmatrix} k_1 & -k_1 \\ -k_1 & k_1 + k_2/\tau^2 \end{bmatrix}\begin{Bmatrix} \vartheta_1 \\ \vartheta_2 \end{Bmatrix} = \begin{Bmatrix} T_M \\ 0 \end{Bmatrix} \qquad (19)$$

Similarly, as explained for the DMF case study, the transfer function correlating the two measures, the input torque and the angular position of the motor shaft, is:

$$\frac{\vartheta_1}{T_T} = \left(\frac{\vartheta_1}{T_M}\right) / \left\{1 + \left[\left(I_M + \frac{I_T}{2}\right)\Omega^2 - c_M j\Omega\right]\frac{\vartheta_1}{T_M}\right\} \qquad (20)$$

where $\frac{\vartheta_1}{T_M} = G_{1,1}(j\Omega)$ is the first element of the receptance matrix.

VI. Simulation results

A. *Case study #1: the DMF*

The transfer functions derived in the former paragraph are here numerically evaluated, using *Matlab*®, considering the parameters values reported in TABLE 1.

I_1[kg m^2]	0.078	c_1[Nms/rad]	0.1
I_2[kg m^2]	0.152	c_2[Nms/rad]	4
k_1[kNm/rad]	13.3	c_B[Nms/rad]	0.3
k_2[kNm/rad]	0.46	c_M[Nms/rad]	0.3

TABLE 1 - DMF model parameters

A comparison of the transfer functions $\frac{\vartheta_1}{T_M}$ and $\frac{\vartheta_1}{T_T}$ is shown in Fig. 10: passing from the first to the second transfer function, the peak amplitude decreases while the peak frequency increases.

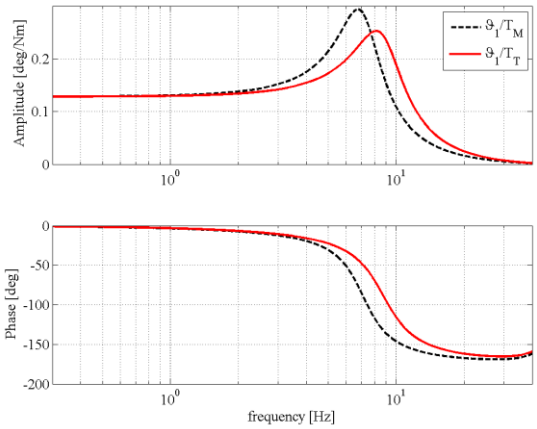

Fig. 10 – Comparison between two transfer functions: the first has the electric motor torque as input, the second has the torque meter torque as input; the output is the same for both, i.e. the motor angular displacement.

In order to validate the results of the 2-DOF torsional dynamic model, the comparison of the experimentally estimated FRF and the modelled FRF calculated through eq. (13) is reported in Fig. 11. The identification of the unknown model parameter, the DMF viscous damping coefficient, was done from the experimental FRF using an iterative curve-fitting algorithm. We observe a very good match between experimental and simulated data especially with reference to the amplitude of the FRF. However, a not negligible difference in phase at low frequency, and also after the resonance, is visible in the lower part of the figure. This is probably due to an inappropriate choice for the damping model of the dual mass flywheel, in fact as stated in [1] the hysteretic damping model is more suitable for characterising the dissipative behaviour of the DMF: the phase lag observed experimentally at low frequency cannot be captured through a viscous damper model.

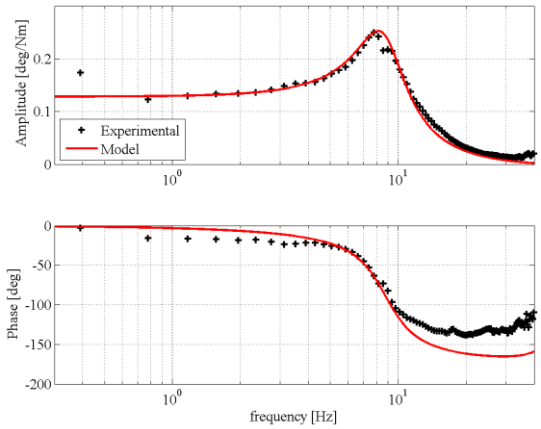

Fig. 11 – Experimental validation of the torsional dynamic model.

B. *Case study #2: the AMT*

Using the numerical values of the parameters shown in TABLE 2 the FRF in eq. (20) has been numerically evaluated for every gear engaged and the model results compared with the experiments.

I_1[kg m^2]	0.23	c_1[Nms/rad]	4
I_2[kg m^2]	0.13	c_O[Nms/rad]	170
k_1[kNm/rad]	0.46	c_B[Nms/rad]	1.5
k_2[kNm/rad]	12.3	c_M[Nms/rad]	0.3
τ_{II}[−]	7.96	τ_{III}[−]	5.42
τ_{IV}[−]	4.14	τ_V[−]	3.26

TABLE 2 - AMT model parameters

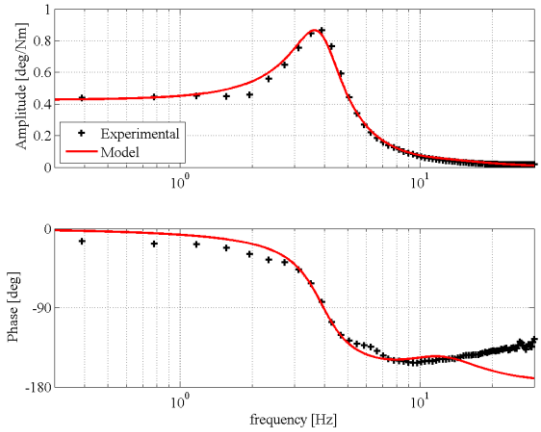

Fig. 12 – Experimental validation of the AMT torsional dynamic model when the 2nd gear is engaged.

As an example, Fig. 12 shows the experimental validation of the model when the transmission has the 2nd gear engaged. A good match is found a part from the phase at high frequencies, where the curves diverge.
The values of the damping coefficients c_O and c_B reported in TABLE 2, representing mainly the damping effect of the gearbox, have been identified through the method of least squares with the aim of getting the best match between model and experiment for the test in 2nd, 3rd and 4th gear, especially regarding the resonance peak.
The experimental test in 5th gear shows a greater damping ratio, 27% compared to 22% of the other tests, hence it was necessary to increase a damping coefficient with respect to its value in the table. A possible choice is to change the value of c_O from 170 to 360 Nms/rad, while leaving unaltered c_B. See [11] for details on how to calculate natural frequencies and damping ratios for a system with non-proportional damping.
Moreover, it must be considered that the oil viscous damping is a function of both the temperature and the Reynold number, therefore changes in oil temperature and gear rotational speed can produce significant differences in the damping effect of the gearbox.
A chart similar to the one reported in Fig. 6, but containing the results of simulations instead of the experimental estimates of the FRF, is shown in Fig.13. The effect of gear ratio on the system dynamic performance is very well described by the although essential torsional model here adopted.

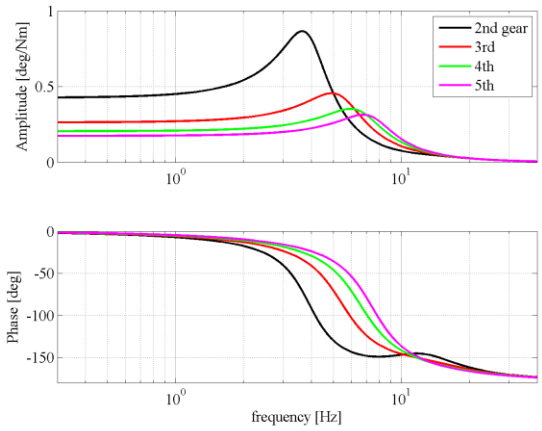

Fig. 13 – AMT simulation results: the effect of the gear ratio on the FRF.

V. Conclusions

In this paper the experimental and analytical methodologies for characterizing the torsional dynamic behaviour of an Automated Manual Transmission and a Dual Mass Flywheel were discussed.
Time-frequency analysis of the torque measures on the test rig revealed two kinds of non-ideality of the torsional exciter: a frequency dependent gain of the torque control system in the pass band and a considerable harmonic distortion.
The compliance FRF have a unique peak in the analysed frequency range for both the case studies. For the AMT, the resonance frequency increases as the gear engaged, from 4Hz in 2nd gear to 7 Hz in 5th gear, gaining about 1 Hz for each gear change.
On the contrary, DC gain decreases approximately in such a way that the ratio between two DC gains is equal to the ratio between the corresponding gear ratios.
The analytical models presented in the paper succeeded in predicting the dynamic behaviour of the analysed transmission system and component in the frequency range considered.
The classical approach for the computation of the FRF from the dynamic system matrices was extended to the case in which the measuring point of the excitation does not coincides with the exact point of application.

References

[1] Galvagno E., Velardocchia M., Vigliani A. and Tota A., Experimental Analysis and Model Validation of a Dual Mass Flywheel for Passenger Cars, SAE Paper Nr. 2015-01-1121, SAE Word Congress 2015, pages 1-8, Detroit (MI), USA, April 21-23, 2015.
[2] Haddow A. G., & Shaw S. W. (2001). Torsional vibration absorbers: A testing and evaluation apparatus (No. 2001-01-1577). SAE Technical Paper.
[3] Mendes A. and Meirelles P., Application of the Hardware-in-the-Loop Technique to an Elastomeric Torsional Vibration Damper, SAE Int. J. Engines 6(4), pages 2004-2014, 2013, doi:10.4271/2013-01-9044.
[4] Sorniotti A., D'Alfio N., Galvagno E., Morgando A., & Amisano F. (2006). Hardware-In-the-Loop Testing of Automotive Control Systems (No. 2006-01-1962). SAE Technical Paper, pages 1-14.
[5] Bracco G., Giorcelli E., Mattiazzo G., Orlando V., & Raffero M. (2014). Hardware-In-the-Loop test rig for the ISWEC wave energy system. Mechatronics, doi:10.1016/j.mechatronics.2014.10.007, pages 11-17.
[6] Williams, J. (1996). Improved methods for digital measurement of torsional vibration (No. 962204). SAE Technical Paper, pages 1-8.
[7] Adamson, S. (2004). Improved approaches to the measurement and analysis of torsional vibration (No. 2004-01-1723). SAE Technical Paper.
[8] Naunheimer H., Bertsche B., Ryborz J., Novak W., "Automotive Transmissions - Fundamentals, Selection, Design and Application", Springer, 2011.
[9] Brandt A., "Noise and Vibration Analysis - Signal Analysis and Experimental Procedures", 2010 John Wiley & Sons, Ltd., ISBN: 978-0-470-74644-8.
[10] Meirovitch L., Fundamentals of Vibrations, McGrawHill, International Edition 2001, ISBN 0-07-118174-1.
[11] Lallement G., Inman D. J., A Tutorial On Complex Eigenvalues, IMAC XIII - 13th International Modal Analysis Conference, Society for Experimental Mechanics, pages 490-495, Nashville, TN, 1995.